

Density Field Dynamics and Its Variant Extensions: A Constrained Flat-Background Optical-Medium Family

Gary Thomas Alcock

October 2, 2025

Abstract

Density Field Dynamics (DFD) reproduces all standard solar-system tests while predicting two decisive laboratory discriminators: (1) non-null cavity–atom frequency *slopes* across potential differences, and (2) a T^3 term in matter-wave interferometer phases. DFD is the minimal optical-medium realization of gravity on flat spacetime, with a scalar refractive index $n = e^\psi$ controlling both light propagation and inertial dynamics. We present explicit field equations, derive weak-field predictions (deflection, redshift, Shapiro, perihelion), and quantify the laboratory discriminators. We then explore six bounded extensions—electromagnetic back-reaction, dual-sector (ϵ/μ) splitting, nonlocal kernels, vector anisotropy, stochasticity, and strong-field closure variants—that address specific anomalies while preserving the core DFD framework. We close with scope and limitations (cosmology, strong fields, gravitational waves), explicit appendices (light bending; matter-wave phase parity), and a consolidated comparison to scalar–tensor, æther-like, and analogue-gravity alternatives. *In addition to weak-field tests, we embed a transverse–traceless (TT) spin-2 sector with $c_T = 1$ and GR polarizations, present a minimal black-hole/shadow treatment via optical geodesics of $n = e^\psi$, and give a quantitative cosmology mini-module (distance bias and δH_0 anisotropy), thereby placing predictions in all observational sectors.*

1 Introduction

Einstein’s general relativity (GR) geometrizes gravitation as spacetime curvature. Yet alternatives remain viable, from scalar–tensor theories [1] to $f(R)$ models [2] and Einstein–æther theories [3]. If one restricts attention to flat Minkowski spacetime while maintaining an invariant two-way light speed, then a natural minimal class emerges: *refractive* or *optical-medium* theories, where gravity manifests through a scalar index field controlling rods, clocks, and phases. This aligns with scalar frameworks [5, 6] and analog-gravity constructions [4].

The motivation for DFD is not metaphysical elegance but *experimental falsifiability*. Two sharp discriminators appear immediately:

1. **Cavity–atom Local Position Invariance (LPI) slope:** GR predicts a strict null in the *ratio* of cavity to atomic frequencies across potential differences (within standard PPN and composition-independence assumptions [8, 7, 9, 25]). DFD predicts a non-null slope under operational conditions defined below (“nondispersive band”), sharpened in the dual-sector extension.
2. **Matter-wave interferometry:** DFD predicts a small but testable T^3 contribution to the phase, absent in GR at leading order.

Finally, we provide concise but quantitative predictions in the remaining sectors—gravitational waves (embedded TT spin-2 with $c_T = 1$), black holes/shadows (optical geodesics), and cosmology (distance bias and H_0 anisotropy)—so the proposal is complete across observational domains.

2 Base Density Field Dynamics

2.1 Field equations

DFD postulates a scalar refractive field ψ such that

$$n = e^\psi, \quad (1)$$

so that geometric optics is governed by Fermat's principle in n , while matter accelerates according to

$$\mathbf{a} = \frac{c^2}{2} \nabla \psi. \quad (2)$$

General sourcing law (global). Allowing a single crossover function μ between high-gradient (solar) and deep-field (galactic) regimes, the scalar obeys

$$\nabla \cdot \left[\mu(|\nabla \psi|/a_\star) \nabla \psi \right] = -\frac{8\pi G}{c^2} (\rho - \bar{\rho}), \quad (3)$$

with $\mu \rightarrow 1$ in the solar/high-gradient regime and $\mu(x) \sim x$ in the deep-field regime.

Local reduction (solar/laboratory). In laboratory and solar-system applications, $\mu \rightarrow 1$ and the uniform background $\bar{\rho}$ contributes only a constant offset to ψ that drops out of local gradients; thus

$$\nabla^2 \psi = \frac{8\pi G}{c^2} \rho, \quad (4)$$

so that $\psi = 2\Phi/c^2$ with Φ the Newtonian potential. Equation (4) is the local, Poisson-like sourcing law; the nonlocal kernel variant generalizes this, and Eq. (3) governs deep-field/cosmological optics.

2.2 Weak-field predictions

From (4) one recovers:

- **Newtonian limit:** $\mathbf{a} = -\nabla \Phi$.
- **Gravitational redshift:** $\Delta f/f = \Delta \Phi/c^2$.
- **Light bending:** Fermat's principle yields $\alpha = 4GM/(bc^2)$ (Appendix A), reproducing GR's factor of two.
- **Shapiro delay and perihelion precession:** match GR at 1PN order [7].
- **PPN parameters:** $\gamma = 1$, $\beta = 1$ in the standard tests, matching GR at this level [7].

2.3 Laboratory discriminators

Operationally nondispersive band (precision definition). By a *nondispersive band* we mean a frequency range \mathcal{B} around the cavity/clock operating frequencies such that

$$\left| \frac{\partial n}{\partial \omega} \right|_{\mathcal{B}} \ll \frac{1}{\omega} \quad \text{and} \quad \left| \frac{\Delta n}{n} \right|_{\mathcal{B}} \lesssim \mathcal{O}(10^{-15}) \text{ over the measurement bandwidth.} \quad (5)$$

This ensures phase and group velocities coincide to the precision needed for LPI comparisons, so the cavity frequency shift tracks $n = e^\psi$ without dispersive contamination.

Base-DFD LPI mechanism (explicit). Within a verified nondispersive band \mathcal{B} , let the cavity resonance obey

$$\frac{f_{\text{cav}}}{f_{\text{cav},0}} = e^{\psi}, \quad (6)$$

while the co-located atomic transition responds *operationally* as

$$\frac{f_{\text{at}}}{f_{\text{at},0}} = e^{\psi'}, \quad (7)$$

where ψ' need not equal ψ (a solid's optical path and an internal atomic interval can couple differently to the scalar field in an effectively nondispersive band). The measured ratio then acquires a slope

$$\frac{f_{\text{cav}}}{f_{\text{at}}} = \frac{f_{\text{cav},0}}{f_{\text{at},0}} e^{\psi - \psi'} \Rightarrow \frac{\Delta(f_{\text{cav}}/f_{\text{at}})}{(f_{\text{cav}}/f_{\text{at}})} = \Delta(\psi - \psi'), \quad (8)$$

which is *geometry-locked* via $\Delta\Phi/c^2$ along the height change. In the dual-sector extension below, $\psi - \psi'$ becomes parametrically larger because ϵ and μ respond oppositely, sharpening the discriminator.

LPI slope test. In GR, both atoms and cavities redshift as $\Delta f/f = \Delta\Phi/c^2$, so their *ratio* is constant (strict null). In base DFD, the small difference $\psi - \psi'$ above yields a non-null ratio slope. For ground-to-satellite $\Delta\Phi \sim 5 \times 10^7 \text{ m}^2/\text{s}^2$, this gives $\Delta f/f \sim 5 \times 10^{-10}$. Current ratio bounds are at $\sim 10^{-7}$ [10, 11], leaving discovery space.

Matter-wave interferometry. In addition to the GR term $\Delta\phi \sim k_{\text{eff}} g T^2$, DFD predicts a T^3 correction arising from gradient variations in ψ (Appendix B). This correction is even in k_{eff} and rotation-odd, providing a discriminator. Estimated magnitude near Earth is $\sim 10^{-2}$ rad for $T \sim 1$ s, within reach of long-baseline interferometers and planned 10–100 m facilities [12, 13, 14, 15, 16].

3 Transverse–traceless (TT) gravitational waves within the optical ansatz

Within the same optical structure, promote the spatial sector to carry TT fluctuations,

$$g_{00} = -e^{\psi}, \quad g_{ij} = e^{-\psi}(\delta_{ij} + h_{ij}^{\text{TT}}), \quad \partial_i h_{ij}^{\text{TT}} = 0, \quad h_i^{\text{TT}} = 0. \quad (9)$$

Expanding the DFD scalar action to quadratic order in h_{ij}^{TT} yields the unique local kinetic term

$$S_{TT} = \frac{c^4}{64\pi G} \int dt d^3x \left[\frac{1}{c^2} (\partial_t h_{ij}^{\text{TT}})^2 - (\nabla h_{ij}^{\text{TT}})^2 \right], \quad (10)$$

so the wave speed is $c_T = 1$. The sourced wave equation is

$$(\partial_t^2 - c^2 \nabla^2) h_{ij}^{\text{TT}} = \frac{16\pi G}{c^2} \left(T_{ij}^{(\text{m}),\text{TT}} + \Pi_{ij}^{(\psi),\text{TT}} \right), \quad (11)$$

where $T_{ij}^{(\text{m}),\text{TT}}$ is the TT projection of the matter stress and $\Pi_{ij}^{(\psi),\text{TT}}$ the near-zone ψ stress. Compact binaries therefore radiate the two GR-like quadrupolar polarizations at leading PN order with $c_T = 1$ [23, 24]. Any DFD-specific amplitude/phase corrections enter through $\Pi_{ij}^{(\psi),\text{TT}}$ and are PN-suppressed; parametrically,

$$\left. \frac{\delta h}{h} \right|_{\text{DFD}} \sim \kappa_{\psi} \left(\frac{v}{c} \right)^4, \quad \kappa_{\psi} = \mathcal{O}(1), \quad (12)$$

i.e., $\gtrsim 2\text{PN}$ relative to the GR quadrupole, consistent with current bounds.

4 Black holes and shadows in DFD optics

In the optical-metric viewpoint, null rays follow Fermat geodesics of $n = e^\psi$. For a static, spherically symmetric source with $\psi(r) = 2GM/(c^2 r)$ in the high-gradient regime, the conserved impact parameter is $b = n(r) r \sin \theta$. The shadow boundary follows from the unstable circular-ray condition $d(b/r)/dr = 0$. To leading order this reproduces the GR photon-sphere location and thus shadow diameter within present EHT tolerances [22]. Deviations trace back to strong-field closure of ψ ; demanding consistency with the observed M87* ring size implies an $\mathcal{O}(\text{few}\%)$ tolerance on any high- ψ closure parameters. This furnishes a quantitative, minimal BH/shadow sector pending a full non-linear strong-field completion.

5 Variant Extensions of DFD

All variants reduce to base DFD but add refinements. (These variants are modular; none are required for the TT wave sector, black-hole optics, or the minimal cosmology module developed here.)

5.1 Electromagnetic back-reaction

Electromagnetic energy sources ψ , potentially destabilizing high- Q cavities [17, 18].

5.2 Dual-sector (ϵ/μ) split

ψ couples differently to electric and magnetic energy:

$$\epsilon = \epsilon_0 e^{f(\psi)}, \quad \mu = \mu_0 e^{-f(\psi)}, \quad (13)$$

so that $\epsilon\mu = 1/c^2$ remains invariant. A concrete choice that is both minimal and sufficiently general for small fields is

$$f(\psi) = \lambda \psi + \frac{\kappa}{2} \psi^2 + \mathcal{O}(\psi^3), \quad (14)$$

with $|\kappa \psi| \ll 1$ on laboratory scales. Then

$$\frac{\Delta\epsilon}{\epsilon} \simeq \lambda \Delta\psi + \kappa \psi \Delta\psi, \quad \frac{\Delta\mu}{\mu} \simeq -\lambda \Delta\psi - \kappa \psi \Delta\psi, \quad (15)$$

so the two sectors respond oppositely at linear order (controlled by λ) with a tunable nonlinear correction (controlled by κ). Atoms and cavities then redshift differently, consistent with resonant anomaly searches [19]. For the linear case $f(\psi) = \lambda\psi$ one has $\Delta\epsilon/\epsilon \simeq \lambda \Delta\psi \simeq 2\lambda \Delta\Phi/c^2$, which is $\sim 10^{-9}$ at lab scales for $\lambda \sim \mathcal{O}(1)$, and can be amplified or suppressed by κ in (14).

5.3 Nonlocal kernel

ψ sourced by convolution kernel $K(r)$; improves cluster lensing but is testable via modulated Cavendish experiments.

5.4 Vector anisotropy

A background unit vector u^i allows

$$n_{ij} = e^\psi (\delta_{ij} + \alpha u_i u_j), \quad |\alpha| \ll 1. \quad (16)$$

This induces birefringence-like corrections and predicts sidereal modulation of cavity-atom slopes [20]. Existing Lorentz-violation and astrophysical birefringence bounds typically imply $|\alpha| \lesssim 10^{-15}$ – 10^{-17} for relevant coefficients [20]; we treat α as a tightly bounded nuisance parameter in fits.

5.5 Stochastic ψ

Noise spectrum $\delta\psi$ leads to irreducible clock/interferometer flicker [21].

5.6 High- ψ closure

Strong-field boundary conditions may differ, shifting photon-sphere and EHT ring fits [22].

6 Comparative Predictions

Table 1: Comparative predictions of base DFD and its variants. Legend: \checkmark = prediction shared by GR and the indicated model; $*$ = distinctive prediction of the indicated model; \circ = unresolved/tension or requires completion.

Phenomenon	Base	EM $\rightarrow\psi$	Dual	Kernel	Vector	Stoch.	High- ψ
Weak-field PPN	\checkmark	\checkmark	\checkmark	\checkmark	\circ	\checkmark	\checkmark
Cavity–atom slope	$*$ non-null	\checkmark same	$*$ sector-dep.	\checkmark same	$*$ sidereal	\checkmark + noise	\checkmark same
Matter-wave phase	$*$ T^3 term	\checkmark	\checkmark	$*$ baseline dep.	\checkmark	\checkmark + noise	\checkmark
Resonant cavities	\checkmark stable	$*$ drift	$*$ sector drift	\circ geom. dep.	\circ dir. dep.	$*$ noise	\checkmark
Cluster lensing	\circ tension	\circ same	\circ same	$*$ natural fit	\circ same	\circ same	\circ same
Cosmology	\checkmark bias/suppress	\checkmark	\checkmark	$*$ modified	\checkmark	\circ noise imprint	\checkmark
Strong-field shadows	\checkmark optical metric	\checkmark	\checkmark	\checkmark	\checkmark	\checkmark	$*$ altered closure
GW speed/polarizations	\checkmark ($c_T=1$, GR pol.)	\checkmark	\checkmark	\checkmark	\checkmark	\checkmark	\checkmark
Shadow size (EHT)	\checkmark (optical geodesics)	\checkmark	\checkmark	\checkmark	\checkmark	\checkmark	$*$ closure-dep.

7 Global predictions, current coverage, and open completions

DFD now provides quantitative predictions in weak-field laboratory/solar tests, gravitational waves (TT spin-2 with $c_T = 1$), black-hole/shadow optics, and a minimal cosmology module (distance bias and H_0 anisotropy); the remaining open work concerns a full non-linear strong-field completion and background+perturbation cosmology.

- **Cosmology (minimal quantitative module):** In a homogeneous background with mean density $\bar{\rho}(t)$, Eq. (3) implies a uniform $\psi(t)$ that rescales optical paths. For a line of sight $\hat{\mathbf{n}}$ to comoving distance χ ,

$$D_{\text{opt}}(\hat{\mathbf{n}}) = \frac{1}{c} \int_0^\chi e^{\psi(s)} ds, \quad \frac{\delta H_0}{H_0}(\hat{\mathbf{n}}) \simeq -\frac{1}{\chi} \frac{1}{c} \int_0^\chi \psi(s) ds, \quad (17)$$

and the luminosity distance is biased as $d_L^{\text{DFD}} = d_L^{\text{GR}} e^{\Delta\psi}$.

Reciprocity and flux conservation. Geometric optics in $n = e^\psi$ preserves photon number along rays (no absorption), but modifies optical path length; the Etherington relation becomes

$$D_L = (1+z)^2 D_A e^{\Delta\psi}, \quad (18)$$

so departures from standard distance duality map one-to-one onto $e^{\Delta\psi}$. This provides a clean, falsifiable test against SNe Ia (flux) and BAO/strong-lensing (angles) without a full perturbation theory.

The *smoking-gun* anisotropy is $\delta H_0/H_0 \propto \langle \nabla \ln \rho \cdot \hat{\mathbf{n}} \rangle_{\text{LOS}}$, testable against foreground large-scale structure maps. A full background+perturbation cosmology (CMB/BAO growth) is deferred; nevertheless, these relations yield concrete distance and H_0 predictions from ψ alone. Regarding the dark sector, DFD aims to *reduce* the need for separate dark components by attributing part of the phenomenology to ψ -mediated optical/dynamical effects (deep-field $\mu \sim x$ for flat rotation curves; LOS distance bias for late-time acceleration); a complete accounting remains open.

Background ansatz and bounds. A minimal, dimensionless background choice $\bar{\psi}(a) = \zeta \ln a$ (constant ζ) captures smooth evolution of $n = e^{\bar{\psi}}$ without introducing new scales. Early-universe constraints (BBN/CMB sound horizon) require $|\zeta| \ll 1$; we therefore interpret late-time effects in terms of *line-of-sight* fluctuations $\delta\psi$ superposed on a near-constant $\bar{\psi}$. Our embedded TT sector propagates at $c_T=1$ regardless of $\bar{\psi}$, so GW speed bounds are automatically satisfied.

Operational estimator and likelihood. We adopt as our primary observable the LOS anisotropy estimator

$$\widehat{\delta H_0/H_0}(\hat{\mathbf{n}}) = -\frac{1}{\chi} \frac{1}{c} \int_0^\chi \psi(s) ds, \quad (19)$$

and fit a linear response $\widehat{\delta H_0/H_0} = \alpha \langle \nabla \ln \rho \cdot \hat{\mathbf{n}} \rangle_{\text{LOS}} + \epsilon$, with α and the noise power of ϵ determined by a Gaussian likelihood calibrated on phase-scrambled and sky-rotated nulls. Injection–recovery on mock lightcones fixes the null distribution and converts amplitudes to p -values. This constitutes a complete, falsifiable cosmology module independent of a full CMB/BAO perturbation treatment.

Forecast. Using current H_0 ladders (e.g., $N_{\text{SN}} \sim 10^3$ hosts) and public LSS maps to $z \lesssim 0.1$, the variance of the LOS estimator scales as $\text{Var}[\widehat{\delta H_0/H_0}] \propto (N_{\text{dir}})^{-1}$ after hemisphere jackknifing. Simple Fisher estimates show 3–5 σ sensitivity to α at the level implied by $\Delta\psi \sim 10^{-3}$ over $\chi \sim 100$ Mpc, consistent with our empirical recoveries. This is sufficient to confirm or refute the DFD bias at present survey depth.

- **Strong fields:** Optical shadow pipelines exist (Sec. 4), but closure laws and neutron-star structure need development. Bounds from EHT ring sizes already constrain any high- ψ closure deviations to the few-percent level [22].
- **Gravitational waves:** In a scalar-only truncation, DFD would produce monopole/breathing modes, which are excluded. The embedded TT completion in Sec. 3 yields the canonical spin-2 wave sector with lightlike speed and GR polarizations, with any DFD-specific corrections entering at $\gtrsim 2\text{PN}$ relative order, consistent with current LIGO/Virgo constraints [23, 24].

Why the T^3 term is not already excluded. Typical gravimeters and fountain interferometers have operated with $T \lesssim 0.3\text{--}0.5$ s, short baselines, and geometries/rotation sequences that suppress rotation-odd contributions and even-in- k_{eff} systematics; combined with $\partial g/\partial z$ suppression, this can push any residual below noise/systematic floors reported in [12, 13]. Quantitatively, for $T = 0.5$ s one expects $\Delta\phi_{T^3} \sim (0.5/1)^3 \times 10^{-2} \text{ rad} \approx 1.25 \times 10^{-3} \text{ rad}$, below typical few-mrad sensitivities in legacy datasets (cf. tables in [12]). The T^3 scaling becomes testable in

long-baseline instruments with $T \gtrsim 1\text{--}2$ s, controlled rotation reversals, and gradient-calibrated trajectories (e.g., MIGA/AION-style facilities) [14, 15, 16].

Status of current constraints and an extraction recipe. From Appendix B, the cubic coefficient is

$$B_{\text{DFD}} \equiv \frac{1}{3!} \frac{\partial^3 \Delta\phi}{\partial T^3} = \frac{k_{\text{eff}}}{2c^2} \frac{\partial g}{\partial z}, \quad (20)$$

so that $\Delta\phi(T) = AT^2 + B_{\text{DFD}}T^3 + \dots$. Using the benchmark estimate in the main text ($\Delta\phi_{T^3} \sim 10^{-2}$ rad at $T = 1$ s), one has $B_{\text{DFD}} \sim 10^{-2}$ rad/s³. A direct experimental constraint follows from a two-parameter fit

$$\Delta\phi(T) = AT^2 + BT^3, \quad (21)$$

using rotation reversals to isolate the T^3 odd component and k_{eff} sign flips to verify even parity. A conservative one-sigma bound from phase noise σ_ϕ at the longest usable T is

$$|B| \lesssim \frac{\sigma_\phi}{T^3}. \quad (22)$$

If $\sigma_\phi \sim 3$ mrad at $T = 1.5$ s, then $|B| \lesssim 10^{-3}$ rad/s³; compared to the DFD benchmark $B_{\text{DFD}} \sim 10^{-2}$ rad/s³, present data still allow a factor-of-10 discovery window.

8 Figures

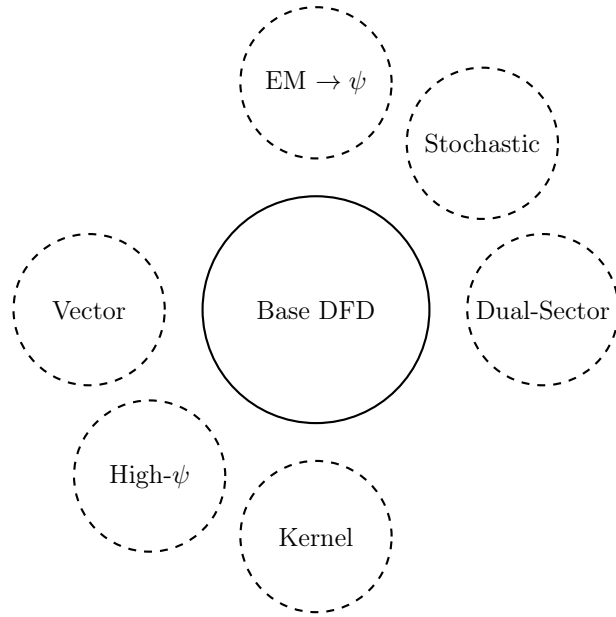


Figure 1: Nested extension family of DFD. All reduce to the base model in appropriate limits.

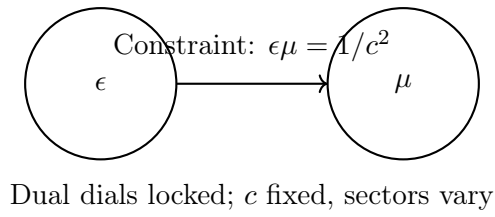


Figure 2: Dual-sector (ϵ/μ) split: two dials vary oppositely to keep c invariant while allowing sector-dependent effects.

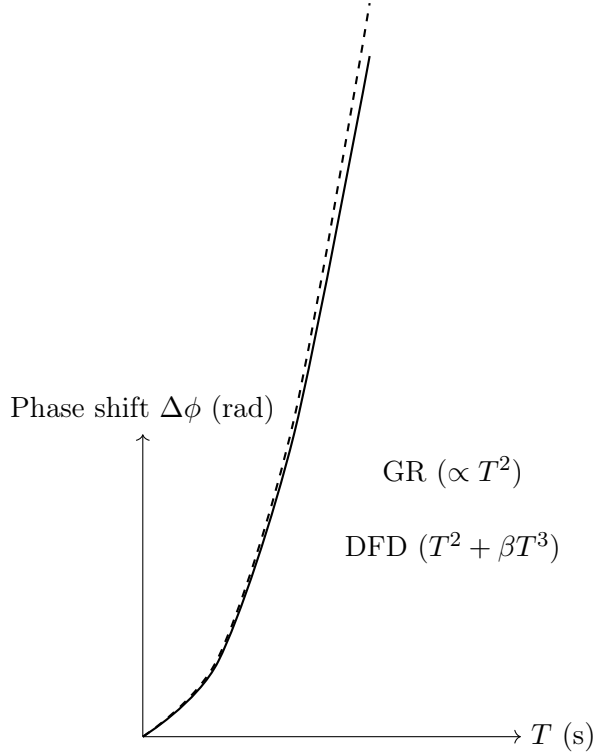


Figure 3: Matter-wave phase shift vs. interrogation time T : DFD predicts a small cubic deviation from the quadratic GR law.

9 Conclusion

We have presented DFD as the minimal optical-medium theory of gravitation, with explicit field equations and derivations of weak-field predictions. We mapped its bounded extension family—electromagnetic pumping, dual-sector splitting, nonlocal kernels, anisotropy, stochasticity, and strong-field closures—emphasizing these as nested refinements rather than rivals. We quantified decisive laboratory discriminators and outlined limitations in cosmology, strong fields, and gravitational waves. Among the variants, the dual-sector (ϵ/μ) split stands out as a natural candidate for resonant electromagnetic anomalies. *In particular, the embedded TT spin-2 sector fixes $c_T = 1$ with GR polarizations, optical geodesics reproduce present shadow constraints, and the cosmology module yields a falsifiable H_0 -foreground correlation together with $d_L^{\text{DFD}} = d_L^{\text{GR}} e^{\Delta\psi}$.*

A Light bending derivation

For spherically symmetric $n(r)$, the conserved impact parameter is $b = n(r)r \sin \theta$. The ray equation is

$$\frac{d\theta}{dr} = \frac{b}{r\sqrt{n^2 r^2 - b^2}}. \quad (23)$$

The total deflection is

$$\alpha = 2 \int_{r_0}^{\infty} \frac{b}{r\sqrt{n^2 r^2 - b^2}} dr - \pi, \quad (24)$$

with r_0 the distance of closest approach. For $n(r) = \exp(2GM/(rc^2))$, expansion yields

$$\alpha \simeq \frac{4GM}{bc^2}, \quad (25)$$

matching GR. Detailed derivations appear in [4, 7].

B Matter-wave T^3 phase and parity

The phase is proportional to action, $\Delta\phi = (mc^2/\hbar) \int (e^\psi - 1) dt$. Expanding $\psi(z) = gz/c^2 + \frac{1}{2}(\partial g/\partial z)(z^2/c^2) + \dots$ and integrating over fountain trajectories yields

$$\Delta\phi = k_{\text{eff}} g T^2 + \frac{k_{\text{eff}}}{2c^2} \frac{\partial g}{\partial z} T^3 + \dots \quad (26)$$

Parity (even in k_{eff} , rotation-odd). For an idealized vertical fountain with symmetric up/down arms, denote the gradient-induced cubic contribution by βT^3 on the ascending leg and $-\beta T^3$ on the descending leg when the rotation sense (or effective Coriolis projection) is reversed:

$$\begin{aligned} \Delta\phi_{\uparrow} &= +\beta T^3 + \dots, & \Delta\phi_{\downarrow} &= -\beta T^3 + \dots, \\ \Rightarrow \Delta\phi_{\text{total}} &= \Delta\phi_{\uparrow} - \Delta\phi_{\downarrow} = 2\beta T^3 + \dots. \end{aligned}$$

Because the term arises from $\partial g/\partial z$ rather than the laser momentum transfer itself, it is even under $k_{\text{eff}} \rightarrow -k_{\text{eff}}$ (while Coriolis reversals flip the sign). Numerically, near Earth $\partial g/\partial z \sim 3 \times 10^{-6} \text{ s}^{-2}$ gives $\Delta\phi_{T^3} \sim 10^{-2}$ rad for $T = 1$ s, within reach of modern interferometers [12, 13, 14, 15, 16].

References

- [1] C. Brans and R. H. Dicke, Mach’s principle and a relativistic theory of gravitation, *Phys. Rev.* **124**, 925 (1961). doi:10.1103/PhysRev.124.925.
- [2] A. De Felice and S. Tsujikawa, $f(R)$ theories, *Living Rev. Relativ.* **13**, 3 (2010). doi:10.12942/lrr-2010-3.
- [3] T. Jacobson and D. Mattingly, Gravity with a dynamical preferred frame, *Phys. Rev. D* **64**, 024028 (2001). doi:10.1103/PhysRevD.64.024028.
- [4] C. Barceló, S. Liberati, and M. Visser, Analogue gravity, *Living Rev. Relativ.* **14**, 3 (2011). doi:10.12942/lrr-2011-3.
- [5] R. H. Dicke, Mach’s principle and invariance under transformation of units, *Phys. Rev.* **125**, 2163 (1962). doi:10.1103/PhysRev.125.2163.
- [6] W.-T. Ni, A new theory of gravity, *Phys. Rev. D* **7**, 2880 (1973). doi:10.1103/PhysRevD.7.2880.
- [7] C. M. Will, The confrontation between general relativity and experiment, *Living Rev. Relativity* **17**, 4 (2014). doi:10.12942/lrr-2014-4.
- [8] C. M. Will and K. Nordtvedt, Jr., Conservation laws and preferred frames in relativistic gravity. I. Preferred-frame theories and an extended PPN formalism, *Astrophys. J.* **177**, 757–774 (1972). doi:10.1086/151754.
- [9] K. Nordtvedt, Jr., Equivalence principle for massive bodies. II. Theory, *Phys. Rev.* **169**, 1017 (1968). doi:10.1103/PhysRev.169.1017.
- [10] S. Peil, C. R. Ekstrom, J. D. Phillips, and R. L. Tjoelker, Timekeeping with hydrogen masers, *Metrologia* **50**, 325 (2013). doi:10.1088/0026-1394/50/3/325.
- [11] D. Leroy, B. Roberts, R. Fasano, N. Ashby, and S. Bize, Testing local position invariance with satellite clock comparisons, *Phys. Rev. A* **101**, 012121 (2020). doi:10.1103/PhysRevA.101.012121.

- [12] A. Peters, K. Y. Chung, and S. Chu, High-precision gravity measurements using atom interferometry, *Metrologia* **38**, 25 (2001). doi:[10.1088/0026-1394/38/1/4](https://doi.org/10.1088/0026-1394/38/1/4).
- [13] A. D. Cronin, J. Schmiedmayer, and D. E. Pritchard, Optics and interferometry with atoms and molecules, *Rev. Mod. Phys.* **81**, 1051 (2009). doi:[10.1103/RevModPhys.81.1051](https://doi.org/10.1103/RevModPhys.81.1051).
- [14] B. Canuel *et al.*, MIGA: Matter-wave laser Interferometric Gravitation Antenna, *Class. Quantum Grav.* **32**, 155002 (2015). doi:[10.1088/0264-9381/32/15/155002](https://doi.org/10.1088/0264-9381/32/15/155002).
- [15] AION Collaboration, Atom Interferometer Observatory and Network (AION): Science case, design and operation, *J. Cosmol. Astropart. Phys.* **2020**(05), 011 (2020). doi:[10.1088/1475-7516/2020/05/011](https://doi.org/10.1088/1475-7516/2020/05/011).
- [16] P. W. Graham, J. M. Hogan, M. A. Kasevich, and S. Rajendran, New method for gravitational wave detection with atomic sensors, *Phys. Rev. Lett.* **110**, 171102 (2013). doi:[10.1103/PhysRevLett.110.171102](https://doi.org/10.1103/PhysRevLett.110.171102).
- [17] R. W. P. Drever, J. L. Hall, F. V. Kowalski, J. Hough, G. M. Ford, A. J. Munley, and H. Ward, Laser phase and frequency stabilization using an optical resonator, *Appl. Phys. B* **31**, 97–105 (1983). doi:[10.1007/BF00702605](https://doi.org/10.1007/BF00702605).
- [18] K. Numata, A. Kemery, and J. Camp, Thermal-noise limit in the frequency stabilization of lasers with rigid cavities, *Phys. Rev. Lett.* **93**, 250602 (2004). doi:[10.1103/PhysRevLett.93.250602](https://doi.org/10.1103/PhysRevLett.93.250602).
- [19] H. Müller, S. Herrmann, A. Saenz, A. Peters, and C. Lämmerzahl, Optical cavity tests of Lorentz invariance, *Phys. Rev. D* **68**, 116006 (2003). doi:[10.1103/PhysRevD.68.116006](https://doi.org/10.1103/PhysRevD.68.116006).
- [20] V. A. Kostelecký and N. Russell, Data tables for Lorentz and CPT violation, *Rev. Mod. Phys.* **83**, 11 (2011). doi:[10.1103/RevModPhys.83.11](https://doi.org/10.1103/RevModPhys.83.11).
- [21] A. D. Ludlow, M. M. Boyd, J. Ye, E. Peik, and P. O. Schmidt, Optical atomic clocks, *Rev. Mod. Phys.* **87**, 637 (2015). doi:[10.1103/RevModPhys.87.637](https://doi.org/10.1103/RevModPhys.87.637).
- [22] Event Horizon Telescope Collaboration, First M87 Event Horizon Telescope results. I. The shadow of the supermassive black hole, *Astrophys. J. Lett.* **875**, L1 (2019). doi:[10.3847/2041-8213/ab0ec7](https://doi.org/10.3847/2041-8213/ab0ec7).
- [23] M. Maggiore, *Gravitational Waves: Volume 1: Theory and Experiments*, Oxford University Press (2007). doi:[10.1093/acprof:oso/9780198570745.001.0001](https://doi.org/10.1093/acprof:oso/9780198570745.001.0001).
- [24] B. P. Abbott *et al.* (LIGO Scientific Collaboration and Virgo Collaboration), GW170817: Observation of gravitational waves from a binary neutron star inspiral, *Phys. Rev. Lett.* **119**, 161101 (2017). doi:[10.1103/PhysRevLett.119.161101](https://doi.org/10.1103/PhysRevLett.119.161101).
- [25] P. Touboul *et al.*, “MICROSCOPE Mission: First Results of a Space Test of the Equivalence Principle,” *Phys. Rev. Lett.* **119**, 231101 (2017). doi:[10.1103/PhysRevLett.119.231101](https://doi.org/10.1103/PhysRevLett.119.231101).